

Article

Thermoluminescent Properties of Cerium-Doped Lu_2SiO_5 and Y_2SiO_5 Single Crystalline Films Scintillators Grown from $\text{PbO-B}_2\text{O}_3$ and Bi_2O_3 Fluxes

Anna Kilian ^{1,*}, Paweł Bilski ¹ , Vitalii Gorbenko ², Tetiana Zorenko ², Sandra Witkiewicz ², Kazimierz Paprocki ²  and Yuriy Zorenko ^{2,*} 

¹ Institute of Nuclear Physics, Polish Academy of Sciences, 31342 Krakow, Poland; pawel.bilski@ifj.edu.pl

² Institute of Physics, Kazimierz Wielki University in Bydgoszcz, 85090 Bydgoszcz, Poland; gorbenko@ukw.edu.pl (V.G.); tzorenko@ukw.edu.pl (T.Z.); s-witkiewicz@wp.pl (S.W.); paprocki@ukw.edu.pl (K.P.)

* Correspondence: anna.kilian@ifj.edu.pl (A.K.); zorenko@ukw.edu.pl (Y.Z.); Tel.: +48-693330869 (Y.Z.)

Received: 8 February 2018; Accepted: 22 February 2018; Published: 4 March 2018

Abstract: In this work we show the influence of material preparation technology on the thermoluminescent properties of single crystalline films (SCFs) of Ce^{3+} -doped Lu_2SiO_5 (LSO) and Y_2SiO_5 (YSO) orthosilicates. LSO:Ce and YSO:Ce SCFs were grown by the liquid phase epitaxy method from two different melt-solutions based on $\text{PbO-B}_2\text{O}_3$ and Bi_2O_3 fluxes. Absorption, cathodoluminescence, and thermoluminescent properties of LSO:Ce and YSO:Ce SCFs grown from the two previously mentioned types of fluxes were compared, and results of spectrally resolved thermoluminescence measurements and thermoluminescent glow curves of SCFs recorded in different spectral ranges were presented. We have found that the observed differences in thermoluminescent properties of the SCFs under study can be caused by the domination of Ce^{4+} and Pb^{2+} emission centers in LSO:Ce and YSO:Ce SCFs grown using $\text{PbO-B}_2\text{O}_3$ flux, and Ce^{3+} and Bi^{3+} emission centers in the SCFs grown from Bi_2O_3 flux.

Keywords: liquid phase epitaxy; single crystalline films; thermoluminescence; Y_2SiO_5 and Lu_2SiO_5 orthosilicates; Ce^{3+} ions; Pb^{2+} and Bi^{3+} flux related dopants

1. Introduction

Lutetium (Lu_2SiO_5 , LSO) and yttrium (Y_2SiO_5 , YSO) orthosilicates are related to the well-known scintillation materials [1]. Due to their high-density, LSO with rare-earth dopants are competitive to other scintillating materials, such as LuAlO_3 (LuAP) perovskite or $\text{Lu}_3\text{Al}_5\text{O}_{12}$ (LuAG) or $\text{Gd}_3\text{Ga}_5\text{O}_{12}$ (GGG) garnets for X-ray imaging with submicron resolution [2,3]. Specifically, during the last few years, Tb^{3+} , Ce^{3+} , and $\text{Ce}^{3+}\text{-Tb}^{3+}$ single crystalline films (SCFs) of LSO and YSO orthosilicates were developed using the liquid phase epitaxy (LPE) method [4–8] for application as scintillating screens in microimaging detectors with special resolution even in the submicron range [9,10].

In our previous works [11–13], we also studied the thermoluminescence (TL) properties of Ce^{3+} -doped LSO and YSO SCFs grown by the LPE method from $\text{PbO-B}_2\text{O}_3$ flux. We have shown that the LSO:Ce and YSO:Ce SCFs exhibit unexpected strong thermoluminescent signal above room temperature (RT) [11–13]. Such promising results led us to further research in this subject. Firstly, it is interesting to determine the nature of trapping centers in Ce^{3+} -doped LSO and YSO SCFs, responsible for such strong thermoluminescence taking into account the absence of substitution-type defects and expected very low concentration of oxygen vacancies in these SCFs due to the very low temperature of their preparation by the LPE method in oxygen-containing atmosphere (air).

In our last works [11–13], we assumed that the formation of such trapping centers in LSO:Ce and YSO:Ce SCFs is related to the use of PbO-based flux and Pt mounting for the crystallization of these films. The nature of these traps is mainly caused by the presence of Pb^{2+} (from flux) and Pt^{4+} (from crucible) contaminations in these SCF samples and the formation of different local charge and volume compensated lattice defects, such as the oxygen or cation vacancies around the mentioned impurities, which can act as trapping centers in the TL of these SCFs [11–13].

On the one hand, the large lead contamination of LSO:Ce and YSO:Ce SCFs in the 0.02–0.19 at.% range (see Table 1) can lead also to the creation of Ce^{4+} - and Pb^{2+} -based centers with local charge and volume compensation, which can also be involved in the TL processes in these SCFs as emission centers [8]. On the other hand, in LSO:Ce and YSO:Ce SCFs grown by the LPE method from Bi_2O_3 flux, mainly the Ce^{3+} valence state is realized in these SCFs in the case of the incorporation of isovalent Bi^{3+} ions as flux agent [8,14,15]. Therefore, in these SCFs we can mainly expect the formation of Bi^{3+} - and Ce^{3+} -based centers [8,15].

Taking these data into account, in this paper we concentrate our attention on the study of the influence of material preparation technology by the LPE method on the TL properties of LSO:Ce and YSO:Ce SCFs. Especially, we compare the influence of different contamination coming to SCFs from $\text{PbO-B}_2\text{O}_3$ or Bi_2O_3 fluxes, used for LPE growth, on the thermoluminescent properties of these SCFs (e.g., the TL glow curve shape and the TL emission spectra).

2. SCF Preparation and Investigation Methods

Nominally undoped and cerium-doped LSO and YSO SCFs were prepared onto undoped YSO substrates (Table 1). The SCFs were grown by the LPE method from a super-cooled melt-solution based on two different fluxes: $\text{PbO-B}_2\text{O}_3$ (samples 1, 2 and 5, 6) and Bi_2O_3 (samples 1, 2 and 5, 6) (Table 1, see also [8,15] for details). The samples were doped with cerium ions using CeO_2 activator with concentration in the 10–20% range. All growth processes were carried out at relatively close growth conditions.

Detailed information about the investigated LSO, YSO, LSO:Ce, and YSO:Ce SCF samples is presented in Table 1. The growth temperatures of LSO- and YSO-based SCFs based on $\text{PbO-B}_2\text{O}_3$ were in the 986–993 °C range. In the case of Bi_2O_3 flux, the LSO and YSO based SCF growth processes were carried out in the 918–945 °C range. The thicknesses of the achieved SCFs were between 6.1 μm (sample 3) and 64 μm (sample 6).

The absorption spectra of the SCFs under study were measured using a Jasco 760 UV-VIS spectrometer (Jasco Int. Co. Ltd, Tokyo, Japan) in the 190–600 nm range. The cathodoluminescence (CL) spectra were investigated at RT using a JSM-820 scanning electron microscope (SEM) (JEOL, Tokyo, Japan), additionally equipped with a StellarNet spectrometer (StellarNet Inc, Tampa, FL, USA) with a thermoelectrically-cooled CCD detector working in the 200–925 nm range.

Measurements of the spectrally resolved thermoluminescence were performed at a set-up based on a SP150 spectrograph (Acton Research Corporation, Acton, MA, USA). The spectral range was 190–1080 nm. The applied heating rate was approximately 0.8 °C/s. Thermal infrared radiation emission was cut off by the use of a KG5 filter with transmittance 300–800 nm (Schott AG, Mainz, Germany). The received spectra were numerically calibrated with respect to wavelength scale and luminescence intensity of the measurement system.

Thermoluminescence was measured using a Risø DA-20 TL/OSL reader (Risø DTU, Roskilde, Denmark) equipped with EMI 9235QB bialkali photomultiplier (sensitivity range approximately 200–600 nm). TL glow curves of all samples were registered from 50 °C to 450 °C. The heating rate was 1 °C/s. Measurements were carried out using two emission band pass filters. The “green” filter Schott BG39 transmits light from 350 to 700 nm. The “UV” Hoya U-340 filter enables measurement in the range of 250 up to 400 nm. Before each irradiation, the samples were annealed in the reader at 450 °C for 10 s.

For both experiments, SCF samples were irradiated with alpha particles. They were exposed to the ^{241}Am source (fluence rate of $1.7 \times 10^5 \text{ cm}^{-2} \cdot \text{s}^{-1}$, energy at samples surface of 5.06 MeV) built-into

the Risø DA-20 TL/OSL reader. The ranges of used alpha particles in LSO and YSO hosts, calculated with SRIM software [14] were 11.7 μm and 13.4 μm , respectively. The thicknesses of SCFs in the investigated samples (see Table 1, column 6) were higher than the estimated ranges of alpha particles in these materials for all samples except for sample 3 (SCF's thickness 6.1 μm). Therefore, we can assume that for the remaining samples the thermoluminescent signal originates only from the SCFs. For sample 3, the TL signal may also be partly emitted from YSO substrate.

Table 1. Growth conditions of the Lu_2SiO_5 (LSO)- and Y_2SiO_5 (YSO)-based single crystalline film (SCF) samples under study. T_g and h are the temperature and the thickness of SCF growth.

ID	Material	Flux	Pb/Bi Content, at %	Ce Content, at %	h , μm	T_g , $^\circ\text{C}$
1	LSO:Ce	PbO- B_2O_3	0.19	0.002	21	990
2	LSO:Ce	Bi_2O_3	2.30	0.032	15	935
3	YSO:Ce	PbO- B_2O_3	0.03	0.052	6.1	983
4	YSO:Ce	Bi_2O_3	0.03	0.002	15	918
5	LSO	PbO- B_2O_3	0.04	-	9	993
6	LSO	Bi_2O_3	1.46	-	64	940
7	YSO	PbO- B_2O_3	0.035	-	15.5	986
8	YSO	Bi_2O_3	1.46	-	10	945

3. Results

3.1. Absorption Spectra

The absorption spectra of the nominally undoped and Ce-doped LSO and YSO SCFs grown from PbO- and Bi_2O_3 -based fluxes are shown in Figure 1a,b, respectively. The characteristic features of the absorption spectra of undoped YSO and LSO SCFs grown from PbO flux are the presence of the intensive bands peaked around 250 nm, 230 nm, and below 200 nm. The intensity of these bands increase with decreasing SCF growth temperature (e.g., the Pb^{2+} content in SCFs), and vice versa. Thus, the mentioned bands are caused by the absorption of Pb^{2+} flux-related impurity. Namely, the bands peaked around 260 nm and <200 nm correspond to the $^1\text{S}_0 \rightarrow ^3\text{P}_1$, $^3\text{P}_2$, and $^1\text{P}_1$ transitions of Pb^{2+} ions (A, B, and C bands), respectively [16]. The latter bands can also be overlapped with the broad bands in the same spectral range related to the charge transfer transition (CTT) between the Pb^{2+} ions and bottom of YSO and LSO conduction bands. The continuous absorption of YSO- and LSO-based SCF samples throughout the whole spectrum up to 800 nm can be caused by the $\text{Pb}^{2+} \rightarrow \text{Pb}^{4+}$ charge transfer transitions [17].

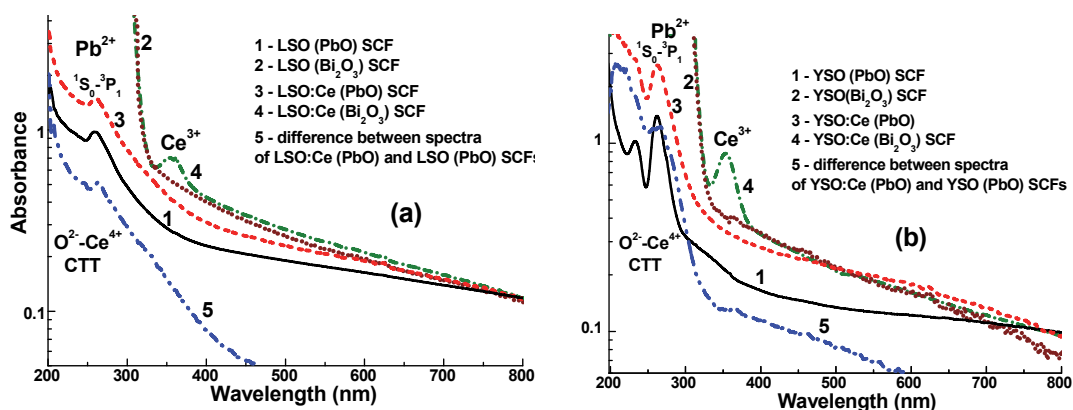


Figure 1. Absorption spectra (in the log scale) of LSO (a) and YSO (b) SCFs (curves 1 and 2) and LSO:Ce (a) and YSO:Ce (b) SCFs (curves 3 and 4), grown from PbO (curves 1 and 2) and Bi_2O_3 (curves 3 and 4) based fluxes. The difference between the spectra of LSO:Ce (PbO) and LSO (PbO) SCFs (curve 5a) and YSO:Ce (PbO) and YSO (PbO) SCFs (curve 5b) shows the presence of $\text{O}^{2-} \rightarrow \text{Ce}^{4+}$ charge transfer transition (CTT) bands in the absorption spectra of LSO:Ce and YSO:Ce SCFs, grown from PbO based flux.

The absorption spectra of YSO:Ce and LSO:Ce SCFs grown from Bi_2O_3 flux are characterized by very strong bands peaked below 320 nm which are related to the $^1\text{S}_0 \rightarrow ^3\text{P}_1$ transitions of Bi^{3+} ions [18]. The large Bi^{3+} concentration (up to 2 at %) in these SCFs can explain the very large intensity of these bands.

Ce^{3+} doping in LSO and YSO SCFs grown from PbO and Bi_2O_3 fluxes yields the additional absorption bands in both the UV and visible ranges (Figures 1a and 2b, curves 2 and 3, respectively). The band peaked at 352 nm—related to the $4f-5d^1$ transitions of Ce^{3+} ions—is well-resolved in the absorption spectra of LSO:Ce and YSO:Ce SCFs grown from the Bi_2O_3 flux; whereas in the spectra of LSO:Ce and YSO:Ce SCFs grown from PbO flux, this band is observed only in the form of small bumps on the low-energy wings of the strong absorption bands related to the transitions of Pb^{2+} ions. Therefore, the main valence state of cerium ions in the last samples is not the Ce^{3+} state. Taking the comparable (by the order of value) cerium and lead content in LSO:Ce and YSO:Ce SCFs (0.03–0.1 at %) into account, we can even suppose the formation of the $\text{Ce}^{4+}\text{-Pb}^{2+}$ pair centers in these SCFs with the local charge and volume compensations.

3.2. Cathodoluminescence (CL) Spectra

The CL spectra of nominally LSO and YSO SCFs grown from Bi_2O_3 flux under excitation with the energy above the band gap of LSO and YSO hosts show two emission bands in the UV and visible ranges (Figure 2a,b, curves 1, respectively). These bands are related to the luminescence of Bi^{3+} -based centers due to contamination from Bi_2O_3 flux, and are typical for the luminescence of Bi^{3+} (ns^2) ions in orthosilicates and other oxide compound hosts [18,19]. The dominant UV bands, peaked at 348 and 340 nm for LSO:Bi and YSO:Bi SCFs, respectively, arise from the $^3\text{P}_{1,0} \rightarrow ^1\text{S}_0$ radiative transitions of Bi^{3+} ions in the seven-fold coordinated Y1/Lu1 cation positions [20–22]. The weaker complex emission bands in the visible range, peaked at 566 nm for LSO:Bi SCFs and at 597 nm for YSO:Bi SCFs at 300 K, probably arise from: (i) the luminescence of the excitons localized around Bi^{3+} ions in YSO and LSO hosts; [18,19] (ii) the intrinsic luminescence of Bi^{2+} centers which are formed under high-energy excitation by way of the capture of an electron by Bi^{3+} ions [23,24].

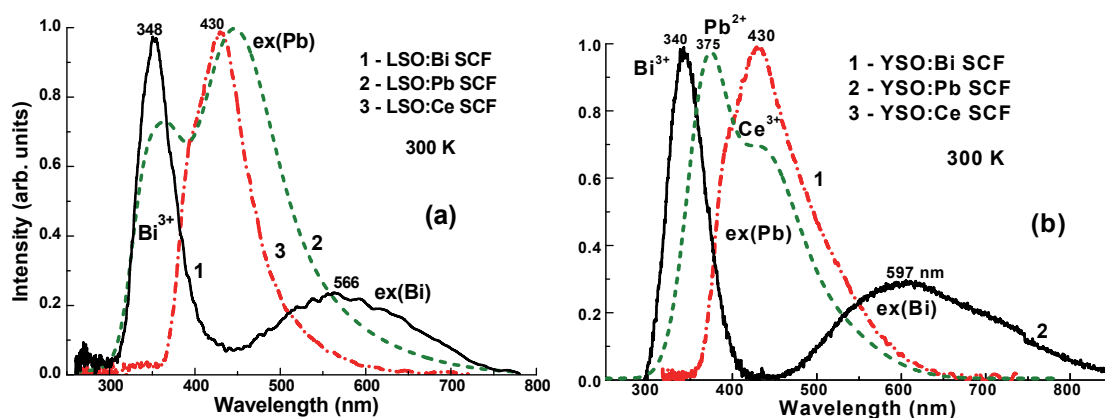


Figure 2. Normalized cathodoluminescence (CL) spectra of nominally undoped (1, 2) and Ce^{3+} -doped (3) (a) LSO SCFs and (b) YSO SCFs at 300 K.

The CL spectra of nominally undoped YSO and LSO SCFs grown from PbO based flux are shown in Figure 2a,b, curves 2, respectively. Both spectra consist of the superposition of the two main UV bands peaked at 374 and 365 nm and two visible bands peaked 434 and 446 nm, respectively. All the mentioned bands are related to the luminescence of Pb^{2+} -based centers due to contamination from PbO-based flux. The emission bands peaked at 374/365 nm correspond to the $^3\text{P}_1 \rightarrow ^1\text{S}_0$ transitions of Pb^{2+} ions in Y1/Lu1 sites of YSO and LSO hosts with seven oxygen ligands [7,16] (further noted as Pb1 centers, respectively). The nature of the 434/446 nm emission bands (Pb2 centers) is still not clear,

and can be interpreted as: (i) the emission of the excitons localized around Pb^{2+} based centers [6–8]; (ii) the luminescence of Pb^{2+} ions in Y1/Lu1 sites of the X2 structure with seven oxygen ligands or in Y2/Lu2 sites of the X1 structure with six oxygen ligands [15,22].

Accounting for the fact that the Pb^{2+} luminescence in LSO and YSO hosts is significantly quenched at room temperature and the Coulomb's compensation is necessary to balance the non-equal Lu^{3+} (Y^{3+}) cation charge state at the embedding of the divalent lead ion, the intensity of the luminescence Pb^{2+} is very small, and its presence in LPE-grown SCFs always leads to a decrease of the luminescence and scintillation efficiency of rare-earth ions—specifically Ce^{3+} ions [15].

On the contrary, the Bi^{3+} ions can be used as activators in LuAG, LSO, and LuAP hosts due to favorable charge state and their dominant intrinsic $^1\text{S}_0 \rightarrow ^3\text{P}_1$ radiative transitions in the UV range [16]. An example is provided in Figure 2, where the CL spectra of LSO and YSO SCFs grown from Bi_2O_3 flux are shown. It is necessary to mention that the photoelectron yield in the Bi-doped LSO and YSO SCFs shows values lower by several times [16] compared with the SCF counterparts grown from PbO -based flux.

The CL spectra of Ce doped LSO and YSO SCFs grown from Bi_2O_3 flux are shown in Figure 2a,b, curves 3, respectively. The dominant doublet emission band peaking around 430 nm in spectra of both YSO:Ce and LSO:Ce SCFs is caused by the Ce^{3+} ions in the positions of Y1 and Lu1 cations with seven oxygen ligands (Ce1 centers). At the same time, some enhancement of these emission bands at the long-wavelength side can be caused by the luminescence of Ce^{3+} ions in the Y2 and Lu2 positions of YSP and LSO hosts with six oxygen ligands (Ce2 centers) [25,26].

3.3. Spectrally-Resolved Thermoluminescence

LSO:Ce and YSO:Ce SCF samples grown from both fluxes were annealed at 400 °C for 30 min and then exposed to alpha particles (at fluence of $6.95 \times 10^9 \text{ cm}^{-2}$). Emission spectra of each sample were collected 3 to 5 days after irradiation. The registered emission spectra were integrated over the whole temperature range.

The comparison of the thermoluminescence emission spectra of both LSO:Ce and YSO:Ce SCFs grown using PbO - B_2O_3 - and Bi_2O_3 -based fluxes is presented in Figure 3. For all measured samples, a peak at 420 nm is dominant within the TL emission spectra. This peak may be associated with the luminescence of Ce^{3+} centers. LSO:Ce and YSO:Ce SCFs prepared with Bi_2O_3 flux also possess an additional luminescence band peaked at 500–600 nm. The enhanced TL emission spectra of these SCF samples with the additional bands peaked at 505 and 492 nm (Figure 3a,b, respectively) are most probably related to the luminescence of the Bi^{3+} -based centers in the complex emission bands in the visible range, namely to the luminescence of the localized excitons around Bi^{3+} single and pair centers or to the luminescence of Bi^{2+} centers [15,18,19]. It is interesting to note here that the UV emission bands—related to the intrinsic $^3\text{P}_{1,0} \rightarrow ^1\text{S}_0$ radiative transitions of Bi^{3+} ions—are fully absent in the TL emission spectra. This can be an additional indication of the different nature of the UV and visible emission bands of Bi^{3+} ions. Namely, the presence of the CL and thermoluminescence of LSO:Ce and YSO:Ce SCFs in the visible band presuppose the recombination nature of such emission (e.g., the subsequent processes of creation e/h pairs, their trapping, and recombination around Bi^{3+} centers).

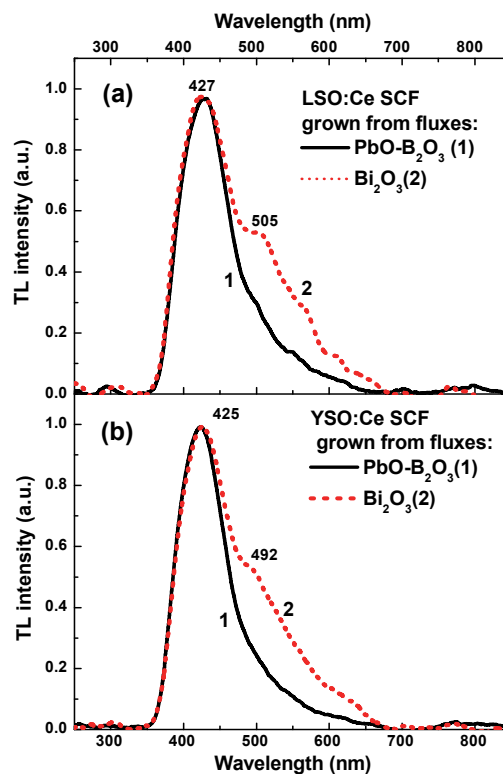


Figure 3. Normalized emission spectra of (a) LSO:Ce and (b) YSO:Ce, prepared with $\text{PbO-B}_2\text{O}_3$ (1) and Bi_2O_3 (2) fluxes, irradiated with alpha particles ($6.95 \times 10^9 \text{ cm}^{-2}$). Emission spectra were integrated over the whole temperature range. TL: thermoluminescence.

3.4. Thermoluminescence Glow Curves

Thermoluminescence glow curves of the investigated samples were collected immediately after irradiation, which was preceded by an annealing process. The doses used for TL readouts with two applied band pass filters were not the same, due to different signal intensities. For measurements in the “UV” range (filter Hoya U-340), samples were exposed to alpha particles with a fluence of $4.08 \times 10^7 \text{ cm}^{-2}$ or beta particles with dose of 6.66 Gy. As a “green” filter’s transmittance (350–700 nm) is better matched to samples’ emission spectra, the dose used was ten times lower than in “UV” range measurements (an alpha fluence of $4.08 \times 10^6 \text{ cm}^{-2}$, a beta dose of 0.67 Gy). Figures 4 and 5 present thermoluminescence glow curves of LSO:Ce and YSO:Ce SCF samples collected using (a) Schott BG39 (“green” range) and (b) Hoya U-340 (“UV” range) emission filters. The inset graphs show corresponding TL glow curves measured after beta irradiation. Because of different samples’ sizes, the registered TL signals were normalized to SCFs’ surface area in the case of alpha irradiation or samples’ masses in the case of beta irradiation.

As can be seen from Figure 4, LSO:Ce SCFs show a significant signal in the above room temperature range. For all samples, two separate TL peaks can be distinguished. The first peak, with the highest intensity, is positioned at around 405 K (132 °C), and the second one at approximately 460 K (187 °C). LSO:Ce SCF sample grown from Bi_2O_3 flux possess more enhanced TL signal—an additional peak at 360 K (87 °C) is observed. Because this peak occurs only in the glow curves of LSO:Ce SCFs grown from Bi_2O_3 flux we can suspect that this part of the signal originates from the centers related to Bi^{3+} ions. The TL measurements conducted with the “green” filter exactly match the emission spectrum of the samples (350–700 nm). Readouts using the “UV” emission filter cover only a part of the spectrum below 400 nm. The shapes of TL glow curves registered under both filters are similar. However, it can be noticed that the intensity of the low-temperature peak (360 K) of SCF samples grown from Bi_2O_3 based flux is relatively higher than that in the TL glow curve registered

with UV filter. This is not observed in thermoluminescence spectra, probably because of high fading of this peak. The spectrally-resolved TL measurements took place a few days after exposure, so this unstable peak decayed.

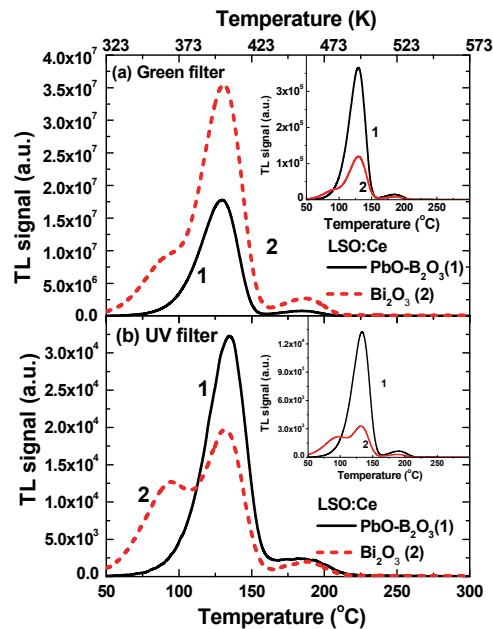


Figure 4. TL glow curves of LSO:Ce SCFs grown from PbO (1) and Bi₂O₃ (2) based fluxes, registered using (a) “green” and (b) “UV” emission filters. Main graphs show TL glow curves measured after irradiation with alpha particles ($3.9 \times 10^7 \text{ cm}^{-2}$) and insets show TL glow curves after exposure to beta particles.

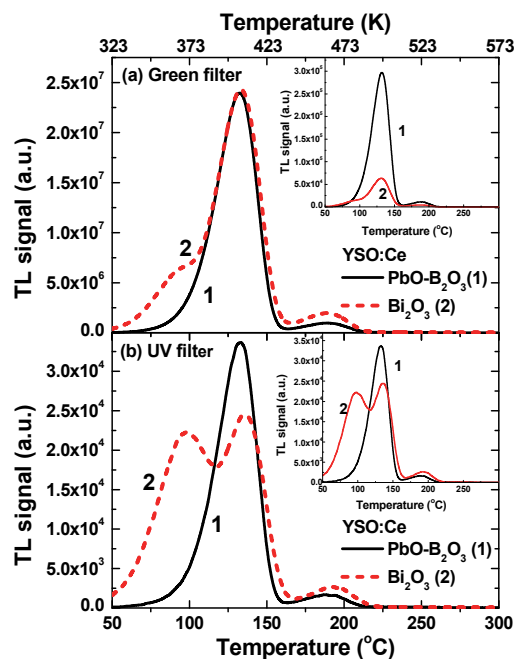


Figure 5. TL glow curves of YSO:Ce SCFs, grown from PbO (1) and Bi₂O₃ (2) based fluxes, registered using (a) “green” and (b) “UV” emission filter. Main graphs show TL glow curves measured after irradiation with alpha particles ($3.9 \times 10^7 \text{ cm}^{-2}$) and insets show TL glow curves after exposure to beta particles.

Figure 5 presents thermoluminescence glow curves of YSO:Ce SCF samples. Sub-graphs show comparison of YSO:Ce TL signal registered with “green” (a) and “UV” (b) emission filters. In the case of YSO:Ce SCF, we can observe similar effects as in the case of LSO:Ce SCF samples. For all the crystals, we can easily distinguish at least two peaks positioned at approximately 407 K (134 °C) and 462 K (189 °C). For (Lu,Y)SO:Ce samples, proportions between the first and second peaks are similar for the same fluxes. For LSO:Ce and YSO:Ce SCF samples, we can also observe the effect of relative increase of low-temperature peak intensity, when measuring in the UV range. In the case of YSO:Ce SCF, this difference is higher—for sample 4, the peak at 365 K became comparable with the peak at 410 K. For LSO:Ce SCFs grown from Bi_2O_3 flux, thermoluminescence intensity is larger in comparison with their $\text{PbO-B}_2\text{O}_3$ -based SCF counterparts. For YSO:Ce SCFs grown from both fluxes, the TL intensity in the main glow peak at 410 K are comparable.

For a more detailed comparison of the obtained TL glow curves, they were deconvoluted into individual peaks. For this purpose, GlowFit software was used [27]. An example of such deconvolution for YSO:Ce samples is shown in Figure 6. Complex results are presented in Table 2. The calculated trap depth energies of two easily distinguishable peaks were similar for the samples grown with the same flux. For the samples grown with the flux based on $\text{PbO-B}_2\text{O}_3$, the trap energies were approximately 1.10 and 1.25 eV, and for the samples prepared with Bi_2O_3 fluxes they were 1.00 and 1.17 eV. For both materials, the existence of a third peak placed in temperatures above 470 K was discovered. The third peak in YSO:Ce SCF samples is shifted towards higher temperatures (~ 509 K) in comparison with LSO SCF (~ 476 K). For this peak, the calculated energy also differed significantly in the materials under study: 0.51 eV for LSO:Ce and 0.87 eV for YSO:Ce. SCFs grown from fluxes based on Bi_2O_3 —both LSO:Ce and YSO:Ce SCFs—possess an additional peak placed around 362 K. For both materials, the trap depth energies are also similar and amount to 0.88 eV. This result also confirms the hypothesis about the Bi^{3+} center origin of this peak.

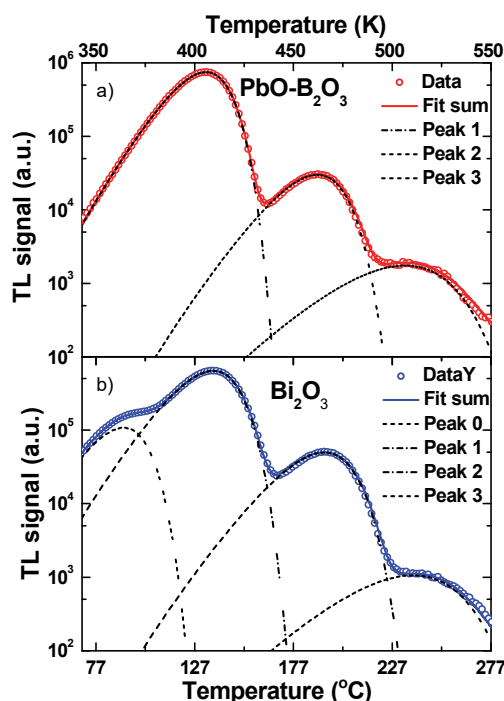


Figure 6. Deconvolution of TL glow curves, registered with “green” emission filter, in YSO:Ce SCF, grown using (a) $\text{PbO-B}_2\text{O}_3$ and (b) Bi_2O_3 fluxes.

Table 2. Parameters of individual TL peaks of LSO:Ce and YSO:Ce SCFs obtained after deconvolution. Relative intensity shows the intensity of a particular peak with respect to peak with maximum intensity.

ID	Peak 0			Peak 1			Peak 2			Peak 3		
	Relative Intensity (%)	T _{max} (K)	E (eV)	Relative Intensity (%)	T _{max} (K)	E (eV)	Relative Intensity (%)	T _{max} (K)	E (eV)	Relative Intensity (%)	T _{max} (K)	E (eV)
1	-	-	-	100	403	1.11	4.1	458	1.29	0.18	478	0.52
2	17	360	0.88	100	404	1.00	7.4	459	1.18	0.14	474	0.50
3	-	-	-	100	406	1.10	4.0	462	1.23	0.23	507	0.87
4	17	364	0.87	100	409	1.01	7.8	466	1.16	0.17	510	0.87

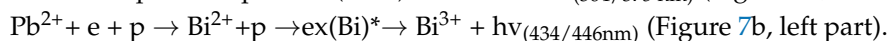
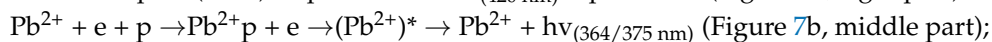
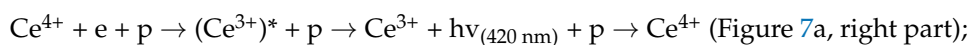
TL glow curves of all the investigated samples were also read after exposure to beta particles. The obtained TL glow curves are presented in the corresponding insets of graphs in Figures 4 and 5. In this case, due to higher penetration of beta radiation [28], registered thermoluminescent signal originates not only from SCFs, but also from the substrates. TL signal from YSO substrates dominates over the measured glow curves, due to larger mass of the substrate in comparison with SCF. For this reason, the effects observed for alpha exposure are not visible in this case.

The observed difference in the TL glow curves under alpha and beta particle radiation can in principle be used for the creation of hybrid film–substrate detectors based on the epitaxial structures of LSO:Ce or YSO:Ce for simultaneous registration of the different components of mixed ionization fluxes. In these types of detectors, the separation of the signal coming from the film and substrate parts can be performed using the differences in peak positions of their TL glow curves.

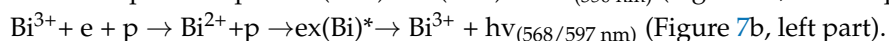
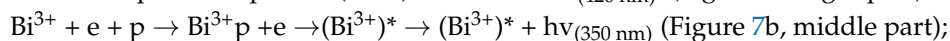
4. Discussion

The above-described differences in the thermoluminescent properties of LSO:Ce and YSO:Ce SCFs prepared from PbO-B₂O₃ and Bi₂O₃ fluxes most likely result from the differences in the type and concentration of main emission centers. Namely, Ce⁴⁺ and Pb²⁺ absorption/emission centers were dominant for LSO and YSO SCFs grown from PbO-B₂O₃ flux (Figures 1a and 2a), while the Ce³⁺ and Bi³⁺ absorption/emission centers were dominant in the SCFs grown from Bi₂O₃ flux (Figure 2b) (see also [8,15]). This could have caused the difference in the TL emission spectra presented in Figure 3. At the same time, due to the different valence state of cerium ions in these SCFs, the recombination processes at Ce ions take place by way of different mechanisms (Figure 7); see also [29,30] and reference therein:

- in (Lu,Y)SO:Ce SCF, grown from PbO-B₂O₃ flux (Figure 7a):



- in (Lu,Y)SO:Ce SCF, grown from Bi₂O₃ flux (Figure 7b):



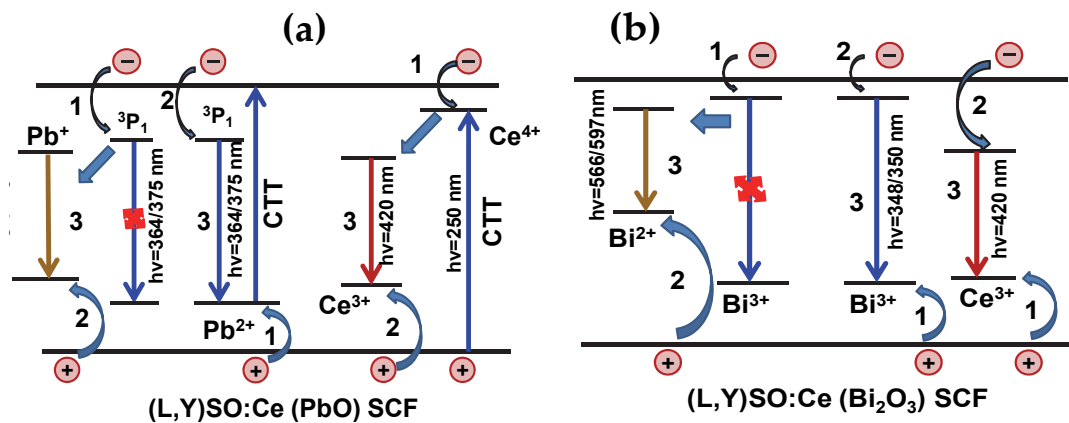


Figure 7. Difference in mechanisms of excitation of the luminescence of Ce⁴⁺ and Ce⁴⁺ centers as well as Pb²⁺ and Bi³⁺ centers in LSO:Ce and YSO:Ce SCFs grown from (a) PbO and (b) Bi₂O₃ based fluxes, respectively.

As can be seen from Figures 4 and 5, the difference in the structure of trapping centers in LSO:Ce and YSO:Ce grown from PbO-B₂O₃ and Bi₂O₃ fluxes is mainly connected with the presence of additional low-temperature peaks at 360–364 °C in (Lu,Y)SO:Ce (Bi₂O₃) SCF samples (Table 2). At the same time, the intensity of the overall TL signal in both SCF samples was caused by the concentration of cerium emitting centers and as Pb²⁺ or Bi³⁺ related emission centers as well as the relative luminescence efficiency of these centers. Namely, the significantly largest TL signal (larger by one order of magnitude) was observed in the LSO:Ce (Bi₂O₃) SCFs (Figure 4) with a typical Ce content of 0.032 at.% and highest Bi content of 2.30 at.% (Table 1) in comparison with the YSO:Ce (PbO-B₂O₃) SCFs (Figure 5) with higher Ce content of 0.052 at.% and typical Pb content of 0.03 at.% (Table 1).

5. Conclusions

The thermostimulated luminescent properties of LSO:Ce and YSO:Ce SCF scintillators grown using the LPE method from PbO-B₂O₃- and Bi₂O₃-based fluxes were investigated depending on Ce content in the 0.02–0.052 at.% range, as well as Pb and Bi contents in the 0.03–0.19 at.% and 0.03–2.30 at.% ranges, respectively.

The Ce³⁺-related luminescence band peak (420 nm) dominated in the TL emission spectra both of LSO:Ce and YSO:Ce SCFs. The SCF samples grown using Bi₂O₃ flux also possessed the 500–600 nm emission band related to the visible luminescence of Bi³⁺-based centers. The LSO:Ce and YSO:Ce SCFs grown from Bi₂O₃ flux showed significantly larger intensity of TL (larger by some order of magnitude) in comparison with their SCF counterparts grown from the PbO-B₂O₃-based flux, due to stronger participation of Bi³⁺ emitting centers in the TL properties of these SCF samples.

The observed differences in the TL properties of the two studied types of SCFs were caused by: (i) the presence of an additional peak at 360–365 K in SCF samples grown from Bi₂O₃ flux; (ii) the differences in their main emission centers: the Ce³⁺ and Bi³⁺ centers in LSO:Ce and YSO:Ce SCFs grown from Bi₂O₃ flux, and Ce⁴⁺ and Pb²⁺ centers in SCFs grown from PbO-B₂O₃-based flux; (iii) the largest emission efficiency of Bi³⁺ flux-related centers in comparison with Pb²⁺ flux-related counterparts.

The effects described above were observed only after irradiation with alpha particles (penetration depth below 10–12 μm). The reason is that beta particles have much larger penetration range and therefore signal originates not only from SCFs, but also from the YSO substrates. In principle, the last effect can be used for the separation of the α- and β-particles in the mixed ionizing radiation fluxes with different penetration capacity using a composite SCF-substrate TL detector, grown by the LPE methods.

Acknowledgments: This work was supported by the Ministry of Science and Higher Education of Poland under Invents Plus project No IP2014 048873 and Polish National Science Centre 2016/21/B/ST8/03200 project.

Author Contributions: Anna Kilian and Pawel Bilski performed TL measurements of SCF samples and wrote project of paper, Vitalii Gorbenko performed SCF growth experiments, Tetiana Zorenko performed the measurements of SCF absorption as well as selected the samples for TL measurements, Kazimierz Paprocki performed the measurements of CL spectra, Sandra Witkiewicz calculated the Pb, Bi and Ce content in SCF samples and contributed to the idea of composite TL detector; Yuriy Zorenko analyzed the whole experimental materials and contributed in writing Introduction, SCF growth and Discussion parts as well as Conclusion of the paper.

Conflicts of Interest: The authors declare no conflict of interest.

References

1. Melcher, C.L.; Manente, R.A.; Peterson, C.A.; Schweizer, J.S. Czochralski growth of rare earth oxyorthosilicate single crystals. *J. Cryst. Growth* **1993**, *128*, 1001–1005. [[CrossRef](#)]
2. Martin, T.; Koch, A. Recent development in X-ray imaging with micrometer spatial resolution. *J. Synchrotron Radiat.* **2006**, *13*, 180–194. [[CrossRef](#)]
3. Zorenko, Y.; Gorbenko, V.; Konstankevych, I.; Grinev, B.; Globus, M. Scintillation properties of $\text{Lu}_3\text{Al}_5\text{O}_{12}:\text{Ce}$ single crystalline films. *Nucl. Instrum. Methods Phys. Res. A* **2002**, *486*, 309–314. [[CrossRef](#)]
4. Martin, T.; Douissard, P.-A.; Couchaud, M.; Cecilia, A.; Baumbach, T.; Dupré, K.; Rack, A. LSO-based single crystal film scintillator for synchrotron-based hard X-ray micro-imaging. *IEEE Trans. Nucl. Sci.* **2009**, *56*, 1412–1418. [[CrossRef](#)]
5. Douissard, P.A.; Cecilia, A.; Martin, T.; Chevalier, V.; Couchaud, M.; Baumbach, T.; Dupré, K.; Kühbacher, M.; Rack, A. A novel epitaxially grown LSO-based thin-film scintillator for micro-imaging using hard synchrotron radiation. *J. Synchrotron Radiat.* **2010**, *17*, 571–583. [[CrossRef](#)] [[PubMed](#)]
6. Zorenko, Y.; Nikl, M.; Gorbenko, V.; Savchun, V.; Voznyak, T.; Kucerlova, R.; Sidletskiy, O.; Grynyov, B.; Fedorov, A. Growth and luminescent properties of Lu_2SiO_5 and $\text{Lu}_2\text{SiO}_5:\text{Ce}$ single crystalline films. *Opt. Mater.* **2011**, *33*, 846–852. [[CrossRef](#)]
7. Zorenko, Y.; Gorbenko, V.; Savchyn, V.; Voznyak, T.; Gorbenko, V.V.; Nikl, M.; Mares, J.A.; Sidletskiy, O.; Grynyov, B.; Fedorov, A.; et al. Scintillation and luminescent properties of undoped and Ce^{3+} doped Y_2SiO_5 and Lu_2SiO_5 single crystalline films grown by LPE method. *Opt. Mater.* **2012**, *34*, 1969–1974. [[CrossRef](#)]
8. Zorenko, Y.; Gorbenko, V.; Savchyn, V.; Zorenko, T.; Grynyov, B.; Sidletskiy, O.; Fedorov, A. Growth and luminescent properties of Ce and Ce-Tb doped $(\text{Y,Lu,Gd})_2\text{SiO}_5:\text{Ce}$ single crystalline films. *J. Cryst. Growth* **2014**, *401*, 577–583. [[CrossRef](#)]
9. Douissard, P.A.; Cecilia, A.; Rochet, X.; Chapel, X.; Martin, T.; Van De Kamp, T.; Helfen, L.; Baumbach, T.; Luquot, L.; Xiao, X.; et al. A versatile indirect detector design for hard X-ray microimaging. *J. Instrum.* **2012**, *7*, P09016. [[CrossRef](#)]
10. Cecilia, A.; Rack, A.; Douissard, P.-A.; Martin, T.; dos Santos Rolo, T.; Vagovič, P.; Hamann, E.; van de Kampa, T.; Riedel, A.; Fiederle, M.; et al. LPE grown LSO: Tb scintillator films for high-resolution X-ray imaging applications at synchrotron light sources. *Nucl. Instrum. Methods Phys. Res. A* **2011**, *648*, S321–S323. [[CrossRef](#)]
11. Twardak, A.; Bilski, P.; Zorenko, Y.; Gorbenko, V.; Mandowski, A.; Mandowska, E.; Sidletskiy, O. Comparative study of TSL and OSL properties of LSO and LSO:Ce single crystals and single crystalline films. *Radiat. Meas.* **2013**, *56*, 196–199. [[CrossRef](#)]
12. Bilski, P.; Twardak, A.; Zorenko, Y.; Zorenko, T.; Gorbenko, V.; Mandowska, E.; Mandowski, A.; Sidletskiy, O.; Mares, J. Thermoluminescent properties of undoped and Ce-doped LSO and YSO single crystals and single crystalline films scintillators. *IEEE Trans. Nucl. Sci.* **2014**, *61*, 276–281.
13. Zorenko, Y.; Gorbenko, V.; Bilski, P.; Twardak, A.; Mandowska, E.; Mandowski, A.; Sidletskiy, O. Comparative analysis of the scintillation and thermoluminescent properties of Ce-doped LSO and YSO crystals and films. *Opt. Mater.* **2014**, *36*, 1715–1719. [[CrossRef](#)]
14. Zorenko, Y.; Gorbenko, V.; Zorenko, T.; Malinowski, P.; Jary, V.; Kucerkova, R.; Beitlerova, A.; Mares, J.A.; Nikl, M. Luminescent and scintillation properties of Bi^{3+} doped Y_2SiO_5 and Lu_2SiO_5 single crystalline films. *J. Lumin.* **2014**, *154*, 525–530. [[CrossRef](#)]

15. Zazubovich, S.; Krasnikov, A.; Zorenko, Y.; Gorbenko, V.; Babin, V.; Mihokova, E.; Nikl, M. Luminescence of Pb- and Bi- Related Centers in Aluminum Garnet, Perovskite, and Orthosilicate Single-Crystalline Films. In *Nanocomposite, Ceramic, and Thin Film Scintillators*; Pan Stanford Publishing Pte. Ltd: Singapore, 2016; pp. 227–287, ISBN 978–981–4745–22–2 (Hardcover); ISBN 978–981–4745–23–9 (eBook).
16. Gorbenko, V.; Krasnikov, A.; Mihokova, E.; Nikl, M.; Zazubovich, S.; Zorenko, Y. Luminescence of lead-related centers in single crystalline films of Lu_2SiO_5 . *J. Phys. D Appl. Phys.* **2012**, *45*, 355304. [[CrossRef](#)]
17. Scott, G.B.; Page, J.L. Pb valence in iron garnets. *J. Appl. Phys.* **1977**, *48*, 1342. [[CrossRef](#)]
18. Gorbenko, V.; Krasnikov, A.; Mihokova, E.; Nikl, M.; Zazubovich, S.; Zorenko, Y. Photoluminescence and excited state structure of Bi^{3+} -related centers in $\text{Lu}_2\text{SiO}_5:\text{Bi}$ single crystalline films. *J. Lumin.* **2013**, *134*, 469–476. [[CrossRef](#)]
19. Babin, V.; Gorbenko, V.; Krasnikov, A.; Mihokova, E.; Nikl, M.; Zazubovich, S.; Zorenko, Y. Photoluminescence and excited state structure in Bi^{3+} -doped Y_2SiO_5 single crystalline films. *Radiat. Meas.* **2013**, *56*, 90–93. [[CrossRef](#)]
20. Ilmer, M.; Grabmaier, B.C.; Blasse, G. Luminescence of Bi^{3+} in gallate garnets. *Chem. Mater.* **1994**, *6*, 204–206. [[CrossRef](#)]
21. Lacklinton, D.E.; Scott, G.B.; Page, G.L. Absorption spectra of Bi^{3+} and Fe^{3+} in $\text{Y}_3\text{Ga}_5\text{O}_{12}$. *Solid State Commun.* **1974**, *14*, 861–863. [[CrossRef](#)]
22. Kärner, T.; Laguta, V.V.; Nikl, M.; Shalapska, T.; Zazubovich, S. On the origin of cerium-related centres in lead-containing single crystalline films of $\text{Y}_2\text{SiO}_5:\text{Ce}$ and $\text{Lu}_2\text{SiO}_5:\text{Ce}$. *J. Phys. D Appl. Phys.* **2014**, *47*, 065303. [[CrossRef](#)]
23. Awater, R.H.P.; Dorenbos, P. X-ray Induced Valence Change and Vacuum Referred Binding Energies of Bi^{3+} and Bi^{2+} in $\text{Li}_2\text{BaP}_2\text{O}_7$. *J. Phys. Chem. C* **2016**, *120*, 15114–15188. [[CrossRef](#)]
24. Awater, R.H.P.; Dorenbos, P. Towards a general concentration quenching model of Bi^{3+} luminescence. *J. Lumin.* **2017**, *188*, 487–489. [[CrossRef](#)]
25. Pidol, L.; Bruno Viana, B.; Kahn-Harari, A.; Ferrand, B.; Dorenbos, P.; van Eijk, C.W.E. Scintillation and thermoluminescence properties of $\text{Lu}_2\text{Si}_2\text{O}_7:\text{Ce}^{3+}$ crystals. *Nucl. Instrum. Methods A* **2005**, *537*, 256–260. [[CrossRef](#)]
26. Feng, H.; Jary, V.; Mihokova, E.; Ding, D.; Nikl, M.; Ren, G.; Li, H.; Pan, S.; Beitlerova, A.; Kucerkova, R. Temperature dependence of luminescence characteristics of $\text{Lu}_{2(1-x)}\text{Y}_{2x}\text{SiO}_5:\text{Ce}^{3+}$ scintillator grown by the Czochralski method. *J. Appl. Phys.* **2010**, *108*, 033519–033524. [[CrossRef](#)]
27. Puchalska, M.; Bilski, P. GlowFit—A new tool for thermoluminescence glow-curve deconvolution. *Radiat. Meas.* **2006**, *41*, 659–664. [[CrossRef](#)]
28. Ziegler, J.F.; Ziegler, M.D.; Biersack, J.P. SRIM—The stopping and range of ions in matter. *Nucl. Instrum. Methods B* **2010**, *268*, 1818–1823. [[CrossRef](#)]
29. Nikl, M.; Kamada, K.; Babin, V.; Pejchal, J.; Pilarova, K.; Mihokova, E.; Beitlerova, A.; Bartosiewicz, K.; Kurosawa, S.; Yoshikawa, A. Defect Engineering in Ce-Doped Aluminum Garnet Single Crystal Scintillators. *Cryst. Growth Des.* **2014**, *14*, 4827–4833. [[CrossRef](#)]
30. Nikl, M.; Yoshikawa, A. Recent R&D Trends in Inorganic Single-Crystal Scintillator Materials. *Adv. Opt. Mater.* **2015**, *3*, 463–481.

